Soft Matter

Cite this: *Soft Matter*, 2012, **8**, 7122

www.rsc.org/softmatter

PAPER

Thermo-mechanical modeling of laser-driven non-contact transfer printing: two-dimensional analysis

Rui Li,†[ab] Yuhang Li,†[bc] Chaofeng Lü,[bd] Jizhou Song,[e] Reza Saeidpouraza,[fg] Bo Fang,[c] Yang Zhong,[a] Placid M. Ferreira,[g] John A. Rogers[fg] and Yonggang Huang*[b]

Received 15th February 2012, Accepted 26th April 2012
DOI: 10.1039/c2sm25339a

Transfer printing is an emerging technique for materials assembly and micro-/nano-fabrication. An important emerging variant of this process involves laser-induced impulsive heating to initiate separation at the interface between a soft, elastomeric stamp and hard micro-/nano-materials (*i.e.* inks) on its surface, due to a large mismatch in coefficients of thermal expansion. The result is the active ejection of the inks from the stamp to a spatially separated receiving substrate, thereby representing the printing step. In the following, a thermo-mechanical model is established to analytically obtain the temperature field, and the energy release rate for delamination at the interface between the stamp and ink in the form of a rigid plate. The normalized critical laser pulse time for interfacial delamination depends only on the normalized total heat flux at the interface and the normalized width of the ink structure. This scaling law has been verified by experiments and the finite element method.

1. Introduction

Transfer printing is an emerging technique for materials assembly and micro-/nano-fabrication. Micro-/nano-scale materials, such as wires, membranes, platelets, *etc.*, are retrieved (*i.e.*, picked up) from a growth (donor) substrate *via* an elastomeric stamp, and then printed onto a different (receiver) substrate.[1–16] This technique can be valuable for the construction of unusual test structures for a variety of basic scientific studies, and also for advanced engineering development of systems such as stretchable/flexible semiconductor devices for structural health monitoring,[17] image sensors,[18–21] flexible display,[22–24] deformable circuits,[25,26] flexible inorganic solar cells[27] and LEDs.[28] Here, transfer printing enables integration of high-performance inorganic semiconductor materials, in ultrathin geometries, with substrates of interest, such as sheets of plastic or slabs or rubber. The resulting components are of particular value in biomedical devices such as smart surgical gloves,[29] in biomimetic, curvilinear electronics,[30] bio-dissolvable electronics,[31] monitors for cardiac electrophysiology[32] and ablation therapy,[33] foldable electrode arrays for mapping brain activity,[34] waterproof optoelectronics for diagnostics,[35] and epidermal electronics for health/wellness evaluation and brain–machine interfaces.[36]

There exist several different approaches for transfer printing.

(1) *Kinetically controlled transfer printing*:[1–4,7,9,13] the inks are retrieved at rapid peel rates and then printed at slow rates onto a receiver substrate by a viscoelastic stamp to take advantage of its high and low adhesion strengths at the large and small peeling rates, respectively.

(2) *Surface-relief-assisted transfer printing*:[8,10,15] stamps with suitable surface relief structures (*e.g.*, microtips at the corners) enable pressure controlled switching between large and small surface area contacts with stamps during retrieval and print, respectively.

(3) *Load-enhanced transfer printing*:[5,6,11,12,14] different mechanical loading protocols facilitate large and small adhesion forces during retrieval and printing, respectively.

(4) *Laser-driven non-contact transfer printing*:[16] a laser pulse initiates separation at the adhesive surface due to large thermal mismatch between the stamp and ink. As illustrated in Fig. 1, the process starts with the retrieval of inks from a donor substrate (Fig. 1a and b) with an elastomer (*e.g.*, PDMS). The "inked" stamp is then brought close (a few micrometers) to the receiving substrate (Fig. 1c). A pulsed laser beam, focusing on the stamp–ink interface, causes the active ejection of the inks from the stamp such that they land on the receiving substrate (Fig. 1d).

Fig. 2 shows a schematic of the experimental setup.[16] Radiation from an electronically pulsed 30 W 805 nm laser diode is

[a]*State Key Laboratory of Structural Analysis for Industrial Equipment, Dalian University of Technology, Dalian 116024, China*
[b]*Dept. of Civil and Environ. Eng. and Mech. Eng., Northwestern University, Evanston, IL 60208, USA. E-mail: y-huang@northwestern.edu*
[c]*School of Astronautics, Harbin Institute of Technology, Harbin 150001, China*
[d]*Dept. of Civil Eng. and Soft Matter Res. Center, Zhejiang University, Hangzhou 310058, China*
[e]*Dept. of Mechanical and Aerospace Engineering, University of Miami, Coral Gables, FL 33146, USA*
[f]*Department of Materials Science and Engineering, University of Illinois, Urbana, IL 61801, USA*
[g]*Department of Mechanical Science and Engineering, University of Illinois, Urbana, IL 61801, USA*
† These authors contributed equally.

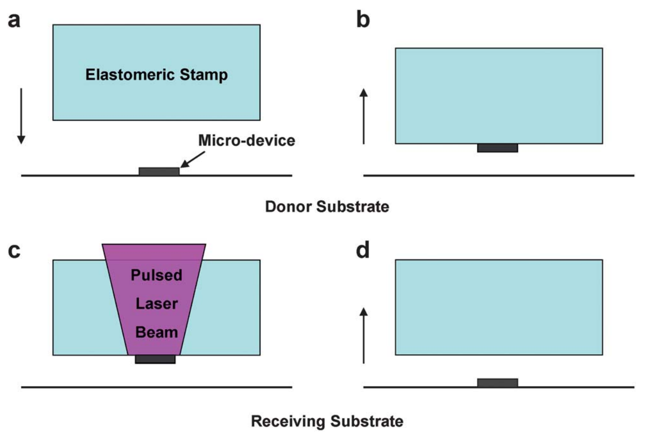

Fig. 1 Schematic illustration of the laser transfer printing process: (a) the PDMS stamp is aligned with a donor substrate to retrieve the ink, illustrated here as a micro-device; (b) the micro-device is lifted onto the surface of the stamp; (c) the stamp is aligned to a receiving substrate and a laser pulse is used to deliver heat to the interface between the micro-device and the stamp; and (d) the micro-device is transferred to the receiving substrate and the stamp is withdrawn for the next printing cycle.

routed through a 250 μm core optical fiber, then collimated and focused to a 400 μm spot at the stamp–ink interface. To obtain the delamination time and the corresponding laser power, the laser pulse duration is set to values of 1, 2, 3 and 4 ms. For each setting, the laser power gradually increases until delamination is achieved. The receiving substrate is then replaced with a photodiode power meter (Thorlabs PM100D). For the same settings of pulse duration and laser power, the energy absorbed by the chip (or the power input to the ink–stamp system) is calculated from measurements of the power at the power meter with and without the ink on the stamp.

A thermo-mechanical model is developed in this paper to identify the mechanisms of laser-driven non-contact transfer printing. It is shown that the mismatch between the thermo-mechanical properties of the stamp and micro-device causes their interfacial delamination. A scaling law is established to identify two non-dimensional combinations of material and geometry parameters that control laser-driven non-contact transfer printing. The finite element method (FEM) is used to validate the simple scaling law, which is useful to the optimal design of a stamp for transfer printing.

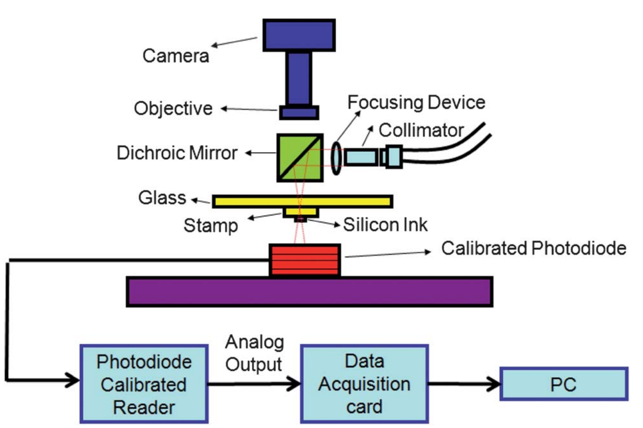

Fig. 2 Laser energy incident on the ink is measured by the difference in energy arriving at a calibrated photodiode with and without the ink present on the stamp.

2. Heat conduction

A heat conduction model is established for the laser-driven non-contact transfer printing illustrated in Fig. 1c. For the ink, or micro-device, we consider a silicon chip with width L_{silicon} and thickness h_{silicon} attached to a PDMS stamp that is much larger than the silicon chip and is modeled as a semi-infinite solid. The total heat flux to the stamp–silicon interface from the pulsed laser beam is denoted by q_{total}. For simplicity, the analysis is two dimensional. The origin of the coordinate system (x,z) is at the center of the stamp–silicon interface, with x along the interface and z pointing into the stamp.

The transient heat conduction equation in the stamp is:[37]

$$\frac{\partial^2\theta_{\text{PDMS}}}{\partial x^2}+\frac{\partial^2\theta_{\text{PDMS}}}{\partial z^2}-\frac{c_{\text{PDMS}}\rho_{\text{PDMS}}}{\lambda_{\text{PDMS}}}\frac{\partial\theta_{\text{PDMS}}}{\partial t}=0 \tag{1}$$

where θ_{PDMS} is the temperature increase from the ambient temperature, t is time, c_{PDMS}, ρ_{PDMS} and λ_{PDMS} are the specific heat, mass density and thermal conductivity of PDMS, respectively. The initial condition is

$$\theta_{\text{PDMS}}|_{t=0}=0. \tag{2}$$

FEM shows that the natural convection on the stamp surface (outside the stamp–silicon interface) is negligible; the insulation boundary condition then gives

$$-\lambda_{\text{PDMS}}\left.\frac{\partial\theta_{\text{PDMS}}}{\partial z}\right|_{z=0}=\begin{cases} q(t) & \text{for } |x|\le L_{\text{silicon}}/2 \\ 0 & \text{for } |x|>L_{\text{silicon}}/2\end{cases}, \tag{3}$$

where $q(t)$ is the heat flux into the stamp.

The temperature increase (from the ambient temperature) in the silicon chip θ_{silicon} is nearly uniform because the thermal conductivity of silicon λ_{silicon} (160 W m^{-1} K^{-1})[38] is three orders of magnitude larger than λ_{PDMS} (0.15 W m^{-1} K^{-1}).[39] Its rate of increase is related to the heat flux into the silicon chip $q_{\text{total}}-q(t)$ by

$$\frac{d\theta_{\text{silicon}}}{dt}=\frac{q_{\text{total}}-q(t)}{c_{\text{silicon}}\rho_{\text{silicon}}h_{\text{silicon}}}, \tag{4}$$

where c_{silicon} and ρ_{silicon} are the specific heat and mass density of silicon, respectively. Continuity of temperature across the stamp–silicon interface requires

$$\theta_{\text{silicon}}=\theta_{\text{PDMS}}|_{z=0} \text{ for } |x|\le L_{\text{silicon}}/2. \tag{5}$$

An approximate solution of $q(t)$ is obtained in the Appendix as

$$q(t)=q_{\text{total}}\left[1-\exp\left(\frac{t}{t_0}\right)\operatorname{erfc}\left(\sqrt{\frac{t}{t_0}}\right)\right], \tag{6}$$

where erfc is the complementary error function,[40] and

$$t_0=\frac{c_{\text{silicon}}^2\rho_{\text{silicon}}^2h_{\text{silicon}}^2}{c_{\text{PDMS}}\rho_{\text{PDMS}}\lambda_{\text{PDMS}}} \tag{7}$$

represents the characteristic time in laser-driven non-contact transfer printing.

The Fourier transform of eqn (1) with respect to x gives a partial differential equation with respect to z and t. The Fourier cosine transform with respect to z, together with the boundary condition (3) and $q(t)$ in eqn (6), gives an ordinary differential equation with respect to t. Its solution, satisfying the initial condition in eqn (2), is obtained analytically. The inverse Fourier transform and inverse Fourier cosine transform give the temperature increase in the stamp as

$$\theta_{\mathrm{PDMS}}(x,z,t)=\frac{c_{\mathrm{silicon}}\rho_{\mathrm{silicon}}h_{\mathrm{silicon}}}{c_{\mathrm{PDMS}}\rho_{\mathrm{PDMS}}\lambda_{\mathrm{PDMS}}}\frac{q_{\mathrm{total}}}{2\sqrt{\pi}}$$

$$\int_0^{t'}\left\{\begin{array}{l}\dfrac{1-\exp(t'-\tau)\mathrm{erfc}\sqrt{t'-\tau}}{\sqrt{\tau}}\exp\left[\dfrac{-z'^2(L'_{\mathrm{silicon}})^2}{4\tau}\right]\times\\ \left[\mathrm{erf}\left(\dfrac{2x'+1}{4\sqrt{\tau}}L'_{\mathrm{silicon}}\right)-\mathrm{erf}\left(\dfrac{2x'-1}{4\sqrt{\tau}}L'_{\mathrm{silicon}}\right)\right]\end{array}\right\}\mathrm{d}\tau \quad (8)$$

where $x' = x/L_{\mathrm{silicon}}$ and $z' = z/L_{\mathrm{silicon}}$ are the normalized coordinates, $t' = t/t_0$ is the normalized time, and

$$L'_{\mathrm{silicon}}=\frac{c_{\mathrm{PDMS}}\rho_{\mathrm{PDMS}}L_{\mathrm{silicon}}}{c_{\mathrm{silicon}}\rho_{\mathrm{silicon}}h_{\mathrm{silicon}}} \quad (9)$$

is the normalized width of the silicon chip, and erf is the error function.[40]

The finite element method is used to obtain the temperature distributions in the stamp and silicon chip. The latter has a length of 100 μm and a thickness of 3 μm, and is modeled as a heat source with the total heat flux q_{total}. The length and thickness of the PDMS are 1000 μm and 300 μm, which yield the same result as that for an infinite PDMS. The continuum element CPE8RT for coupled thermal–mechanical analysis in the ABAQUS package is used.[41]

Eqn (8) suggests that the temperature increase, normalized by $c_{\mathrm{silicon}}\rho_{\mathrm{silicon}}h_{\mathrm{silicon}}q_{\mathrm{total}}/(c_{\mathrm{PDMS}}\rho_{\mathrm{PDMS}}\lambda_{\mathrm{PDMS}})$, depends on the normalized position (x' and z') and time (t'), and a single combination of stamp and silicon chip properties $L'_{\mathrm{silicon}} = c_{\mathrm{PDMS}}\rho_{\mathrm{PDMS}}L_{\mathrm{silicon}}/(c_{\mathrm{silicon}}\rho_{\mathrm{silicon}}h_{\mathrm{silicon}})$. As shown in Fig. 3, the temperature increase in eqn (8), normalized by $c_{\mathrm{silicon}}\rho_{\mathrm{silicon}}h_{\mathrm{silicon}}q_{\mathrm{total}}/(c_{\mathrm{PDMS}}\rho_{\mathrm{PDMS}}\lambda_{\mathrm{PDMS}})$, *versus* $x' = x/L_{\mathrm{silicon}}$ agrees well with that obtained by FEM for $z' = z/L_{\mathrm{silicon}} = 0$, 0.1 and 0.2, and the normalized time $t' = 8.90$ and $L'_{\mathrm{silicon}} = 29.0$, which corresponds to $c_{\mathrm{silicon}} = 708$ J kg^{-1} K^{-1}, $\rho_{\mathrm{silicon}} = 2.30 \times 103$ kg m^{-3},[38] $c_{\mathrm{PDMS}} = 1.46$ kJ kg^{-1} K^{-1}, $\rho_{\mathrm{PDMS}} = 970$ kg m^{-3},[39] $L_{\mathrm{silicon}} = 100$ μm and $h_{\mathrm{silicon}} = 3$ μm in the experiment.[16]

The temperature increase in the silicon chip can be obtained from the continuity at the stamp–silicon interface as

$$\theta_{\mathrm{silicon}}(t)=\frac{c_{\mathrm{silicon}}\rho_{\mathrm{silicon}}h_{\mathrm{silicon}}}{c_{\mathrm{PDMS}}\rho_{\mathrm{PDMS}}\lambda_{\mathrm{PDMS}}}\frac{q_{\mathrm{total}}}{\sqrt{\pi}L'_{\mathrm{silicon}}}\times\int_0^{t'}\left[1-\exp(t'-\tau)\mathrm{erfc}\sqrt{t'-\tau}\right]$$

$$\left\{\frac{L'_{\mathrm{silicon}}}{\sqrt{\tau}}\mathrm{erf}\frac{L'_{\mathrm{silicon}}}{2\sqrt{\tau}}-\frac{2}{\sqrt{\pi}}\left[1-\exp\frac{-(L'_{\mathrm{silicon}})^2}{4\tau}\right]\right\}\mathrm{d}\tau. \quad (10)$$

The normalized temperature increase in the silicon chip, $c_{\mathrm{PDMS}}\rho_{\mathrm{PDMS}}\lambda_{\mathrm{PDMS}}\theta_{\mathrm{silicon}}/(c_{\mathrm{silicon}}\rho_{\mathrm{silicon}}h_{\mathrm{silicon}}q_{\mathrm{total}})$, depends only on the normalized time t' and a single combination of stamp and silicon chip properties $L'_{\mathrm{silicon}} = c_{\mathrm{PDMS}}\rho_{\mathrm{PDMS}}L_{\mathrm{silicon}}/(c_{\mathrm{silicon}}\rho_{\mathrm{silicon}}h_{\mathrm{silicon}})$. This is shown in Fig. 4 for $L'_{\mathrm{silicon}} = 29.0$, which agrees well with the results obtained by FEM.

3. Delamination of the stamp–silicon interface

For plane-strain analysis, the temperature increase in Section 2 yields the in-plane thermal strain $(1 + \nu_{\mathrm{PDMS}})\alpha_{\mathrm{PDMS}}\theta_{\mathrm{PDMS}} = 3\alpha_{\mathrm{PDMS}}\theta_{\mathrm{PDMS}}/2$, which drives delamination of the stamp–silicon interface, where ν_{PDMS} (0.5) is the Poisson's ratio of PDMS, $\alpha_{\mathrm{PDMS}}(3.1 \times 10^{-4}\ \mathrm{K}^{-1})$[39] is the coefficient of thermal expansion (CTE) of PDMS and is two orders of magnitude larger than the CTE of silicon (2.6×10^{-6} K^{-1}),[42] such that the latter is negligible.

Suo[43] obtained the complex stress intensity factor for an interfacial crack tip between two dissimilar materials subjected to a uniform transformation strain within a circular region of radius R. For the interfacial crack tip at $(x_0,0)$ and the circular region in PDMS with the center at (x,z) $(z > 0)$, the complex stress intensity factor is $K^* = \pi R^2\sqrt{2/\pi}\mu_{\mathrm{PDMS}}(\varepsilon^{\mathrm{T}}_{xx}+\varepsilon^{\mathrm{T}}_{zz})(x-x_0-iz)^{-3/2}$,

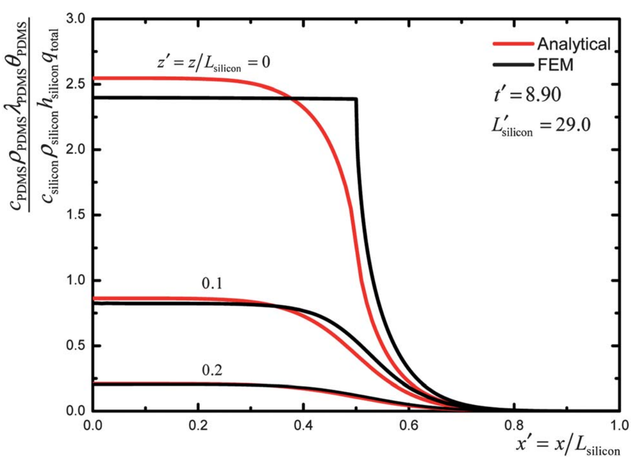

Fig. 3 The distribution of increase in normalized temperature of the stamp.

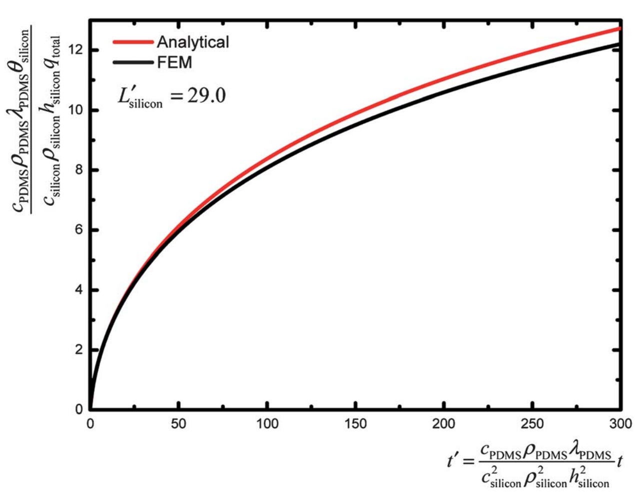

Fig. 4 The normalized temperature increase in the silicon chip.

where i is the imaginary unit, $\varepsilon_{xx}^{\mathrm{T}}$ and $\varepsilon_{zz}^{\mathrm{T}}$ are the transformation strains, the shear modulus of PDMS μ_{PDMS} is five orders of magnitude smaller than that of silicon, and PDMS is nearly incompressible. This gives the stress intensity factor $\sqrt{2/\pi}\mu_{\mathrm{PDMS}}(\varepsilon_{xx}^{\mathrm{T}}+\varepsilon_{zz}^{\mathrm{T}})(x-x_0-iz)^{-3/2}$ for a point dilatation. For thermal strains $\varepsilon_{xx}^{\mathrm{T}} = \varepsilon_{zz}^{\mathrm{T}} = 3\alpha_{\mathrm{PDMS}}\theta_{\mathrm{PDMS}}/2$, the stress intensity factor for the crack tip ($-L_{\mathrm{silicon}}/2$,0) is

$$K = 3\sqrt{\frac{2}{\pi}}\mu_{\mathrm{PDMS}}\alpha_{\mathrm{PDMS}}\int_{z=0}^{\infty}\int_{x=-\infty}^{\infty}\theta_{\mathrm{PDMS}}(x,z,t)\left(x+\frac{L_{\mathrm{silicon}}}{2}-iz\right)^{-3/2}\mathrm{d}x\mathrm{d}z. \tag{11}$$

Substitution of eqn (8) into the above expression gives

The interfacial crack tip energy release rate[43] $G = |K|^2/(8\mu_{\mathrm{PDMS}})$ is given by

$$K = \frac{6\mu_{\mathrm{PDMS}}\alpha_{\mathrm{PDMS}}}{\lambda_{\mathrm{PDMS}}}\sqrt{\frac{2L_{\mathrm{silicon}}^3}{\pi^3}}q_{\mathrm{total}}\int_0^{t'}\frac{\exp(t'-\tau)\mathrm{erfc}\sqrt{t'-\tau}-1}{\tau}\mathrm{d}\tau\int_0^{\infty}\exp\left[\frac{-\eta^2(L'_{\mathrm{silicon}})^2}{4\tau}\right]\mathrm{d}\eta$$
$$\times\int_{-\infty}^{\infty}(\xi-i\eta)^{-1/2}\exp\left[-\frac{(2\xi-1)^2+1}{16\tau}(L'_{\mathrm{silicon}})^2\right]\sin\mathrm{h}\left[\frac{2\xi-1}{8\tau}(L'_{\mathrm{silicon}})^2\right]\mathrm{d}\xi. \tag{12}$$

$$G = 9\mu_{\mathrm{PDMS}}\left(\frac{\alpha_{\mathrm{PDMS}}}{\lambda_{\mathrm{PDMS}}}\right)^2\left(\frac{c_{\mathrm{silicon}}\rho_{\mathrm{silicon}}h_{\mathrm{silicon}}}{\pi c_{\mathrm{PDMS}}\rho_{\mathrm{PDMS}}}\right)^3 q_{\mathrm{total}}^2(L'_{\mathrm{silicon}})^3$$
$$\times\left|\begin{array}{l}\int_0^{t'}\frac{\exp(t'-\tau)\mathrm{erfc}\sqrt{t'-\tau}-1}{\tau}\mathrm{d}\tau\int_0^{\infty}\exp\left[\frac{-\eta^2(L'_{\mathrm{silicon}})^2}{4\tau}\right]\mathrm{d}\eta\\ \times\int_{-\infty}^{\infty}(\xi-i\eta)^{-1/2}\exp\left[-\frac{(2\xi-1)^2+1}{16\tau}(L'_{\mathrm{silicon}})^2\right]\sin\mathrm{h}\left[\frac{2\xi-1}{8\tau}(L'_{\mathrm{silicon}})^2\right]\mathrm{d}\xi\end{array}\right|^2. \tag{13}$$

The energy release rate, normalized by $\mu_{\mathrm{PDMS}}(\alpha_{\mathrm{PDMS}}/\lambda_{\mathrm{PDMS}})^2[c_{\mathrm{silicon}}\rho_{\mathrm{silicon}}h_{\mathrm{silicon}}/(\pi c_{\mathrm{PDMS}}\rho_{\mathrm{PDMS}})]^3 q_{\mathrm{total}}^2$, depends only on the normalized time, t/t_0, and normalized width of the silicon chip, L'_{silicon}.

4. Scaling law for the laser pulse time for delamination

The stamp–silicon interface delaminates when the crack tip energy release rate in eqn (13) reaches the work of adhesion γ of the interface (e.g., 0.15 J m^{-2} for stamp–silicon interface)[16],

$$G = \gamma. \tag{14}$$

Its substitution into eqn (13) gives a scaling law for the critical time $t_{\mathrm{delamination}}$ of stamp–silicon interfacial delamination,

$$\frac{t_{\mathrm{delamination}}}{t_0} = f\left(\frac{q_{\mathrm{total}}}{q_0},\frac{L_{\mathrm{silicon}}}{L_0}\right), \tag{15}$$

where t_0 is given in eqn (7), and

$$q_0 = \frac{\lambda_{\mathrm{PDMS}}}{\alpha_{\mathrm{PDMS}}}\sqrt{\frac{\gamma}{\mu_{\mathrm{PDMS}}}\left(\frac{c_{\mathrm{PDMS}}\rho_{\mathrm{PDMS}}}{c_{\mathrm{silicon}}\rho_{\mathrm{silicon}}h_{\mathrm{silicon}}}\right)^3}, L_0 = \frac{c_{\mathrm{silicon}}\rho_{\mathrm{silicon}}h_{\mathrm{silicon}}}{c_{\mathrm{PDMS}}\rho_{\mathrm{PDMS}}}. \tag{16}$$

The normalized delamination time $t_{\mathrm{delamination}}/t_0$ depends only on two parameters: the normalized total heat flux q_{total}/q_0 and the normalized width of the silicon chip L_{silicon}/L_0. Fig. 5 shows the scaling law in eqn (15), $t_{\mathrm{delamination}}/t_0$ *versus* q_{total}/q_0, for L_{silicon}/L_0 = 3, 5, 10, and 29.0. The laser pulse time of 1, 2, 3 and 4 ms in the experiment correspond to absorbed laser power by the ink (100 × 100 × 3 μm polished SCS squares) 0.0672, 0.0403, 0.0269 and 0.0222 W, respectively, which give the total heat flux 6.72 × 10^6, 4.03 × 10^6, 2.69 × 10^6 and 2.22 × 10^6 W m^{-2}.[16] The results from experiments and FEM, shown in Fig. 5 for L_{silicon}/L_0 = 29.0, agree very well with the analytical model.

5. Discussions and concluding remarks

Laser-driven non-contact transfer printing avoids direct contact between the silicon chip (ink) and receiver substrate, and initiates delamination of the stamp–ink interface by the laser pulse. This is because the stamp and silicon chip have a large mismatch in thermal properties (specific heat, thermal conductivity, and coefficient of thermal expansion) such that the temperature rise due to laser pulse gives a large thermal stress, which drives interfacial delamination.

Laser-driven non-contact transfer printing involves 8 properties of the stamp, silicon chip and their interface: the specific heat c_{PDMS} and c_{silicon}, mass density ρ_{PDMS} and ρ_{silicon}, thermal conductivity λ_{PDMS}, coefficient of thermal expansion α_{PDMS}, shear modulus μ_{PDMS}, and work of adhesion γ of the interface. It

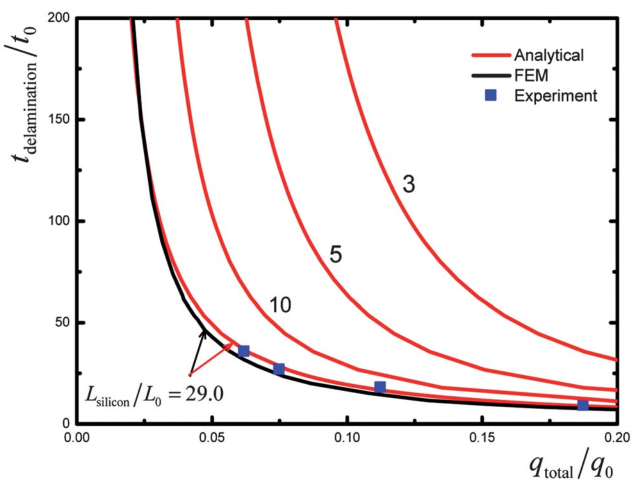

Fig. 5 The scaling law for delamination of the stamp–silicon interface.

also depends on the thickness h_{silicon} and width L_{silicon} of the silicon chip, and the total heat flux to the stamp–silicon interface q_{total} from the pulsed laser beam. The scaling law in eqn (15) shows that the critical laser pulse time $t_{\text{delamination}}$ for stamp–silicon interfacial delamination depends only on the total heat flux q_{total} and width L_{silicon} of the silicon chip. All 8 properties and thickness of the silicon chip only appear to normalize $t_{\text{delamination}}$, q_{total} and L_{silicon}. This scaling law has been verified by experiments and FEM, and gives a critical laser pulse time for the laser-driven non-contact transfer printing.

It should be pointed out that, for a very small silicon chip $L_{\text{silicon}} \ll L_0$, the scaling law in eqn (15) can be obtained analytically as

$$\int_0^{\frac{t_{\text{delamination}}}{t_0}} \frac{1-\exp\left(\frac{t_{\text{delamination}}}{t_0}-\tau\right)\operatorname{erfc}\sqrt{\frac{t_{\text{delamination}}}{t_0}-\tau}}{\tau^{3/4}} \times \mathrm{d}\tau = 3.071\,\frac{\frac{\lambda_{\text{PDMS}}}{\alpha_{\text{PDMS}}}\sqrt{\frac{\gamma}{\mu_{\text{PDMS}}}\frac{c_{\text{PDMS}}\rho_{\text{PDMS}}}{c_{\text{silicon}}\rho_{\text{silicon}}h_{\text{silicon}}}}}{q_{\text{total}}L_{\text{silicon}}}. \quad (17)$$

For a representative total heat flux 6.72×10^6 W m^{-2}, the delamination time is $t_{\text{delamination}} = 4.51$ s, 71.3 s and 4.44×10^4 s for the silicon chip width $L_{\text{silicon}} = 1$ μm, 500 nm and 100 nm, respectively, which are much larger than the laser pulse time (~1 ms) such that, at small silicon chip widths, the stamp–silicon interface may not delaminate during the laser pulse time.

Appendix. Heat flux into the stamp

An approximate heat conduction model $\frac{\partial^2\theta_{\text{PDMS}}}{\partial z^2} - \frac{c_{\text{PDMS}}\rho_{\text{PDMS}}}{\lambda_{\text{PDMS}}}\frac{\partial\theta_{\text{PDMS}}}{\partial t} = 0$ is adopted to estimate the heat flux into the stamp $q(t)$. The Fourier cosine transform $\tilde{\theta}_{\text{PDMS}} = \int_0^\infty \theta_{\text{PDMS}}(z)\cos(\beta z)\mathrm{d}z$, together with the boundary condition in eqn (3), give

$$\frac{c_{\text{PDMS}}\rho_{\text{PDMS}}}{\lambda_{\text{PDMS}}}\frac{\partial\tilde{\theta}_{\text{PDMS}}}{\partial t} + \beta^2\tilde{\theta}_{\text{PDMS}} = \frac{q(t)}{\lambda_{\text{PDMS}}}. \quad (A1)$$

Its solution, satisfying the initial condition in eqn (2), is

$$\tilde{\theta}_{\text{PDMS}}(\beta,t) = \frac{1}{c_{\text{PDMS}}\rho_{\text{PDMS}}}\int_0^t q(\tau)\exp\left[-\frac{\lambda_{\text{PDMS}}\beta^2}{c_{\text{PDMS}}\rho_{\text{PDMS}}}(t-\tau)\right]\mathrm{d}\tau. \quad (A2)$$

The inverse Fourier cosine transform then gives $\theta_{\text{PDMS}}(z=0) = \frac{1}{\sqrt{\pi c_{\text{PDMS}}\rho_{\text{PDMS}}\lambda_{\text{PDMS}}}}\int_0^t \frac{q(\tau)}{\sqrt{t-\tau}}\mathrm{d}\tau$, which also equals θ_{silicon} from the continuity condition in eqn (5). Its substitution into the integral form of eqn (4) yields

$$\frac{1}{\sqrt{\pi c_{\text{PDMS}}\rho_{\text{PDMS}}\lambda_{\text{PDMS}}}}\int_0^t \frac{q(\tau)}{\sqrt{t-\tau}}\mathrm{d}\tau = \frac{1}{c_{\text{silicon}}\rho_{\text{silicon}}h_{\text{silicon}}}\left[q_{\text{total}}t - \int_0^t q(\tau)\mathrm{d}\tau\right]. \quad (A3)$$

The above equation is solved by the Laplace transform, which gives eqn (6).

Acknowledgements

The materials presented here are based upon work supported by the Center for Nanoscale Chemical-Electrical-Mechanical System (NanoCEMMS), a Nanoscale Science and Engineering Center sponsored by NSF under Award #0749028 (CMMI). The support from NSF grants ECCS 0824129 and OISE 1043143 is also acknowledged. Y.H. acknowledges the support from NSFC. C.L. acknowledges the support from NSFC by grant no. 11172263.

References

1 M. A. Meitl, Z. T. Zhu, V. Kumar, K. J. Lee, X. Feng, Y. Y. Huang, I. Adesida, R. G. Nuzzo and J. A. Rogers, *Nat. Mater.*, 2006, **5**, 33–38.
2 X. Feng, M. A. Meitl, A. M. Bowen, Y. Huang, R. G. Nuzzo and J. A. Rogers, *Langmuir*, 2007, **23**, 12555–12560.
3 J. Yu and V. Bulovic, *Appl. Phys. Lett.*, 2007, **91**, 043102.
4 S. I. Park, Y. J. Xiong, R. H. Kim, P. Elvikis, M. Meitl, D. H. Kim, J. Wu, J. Yoon, C. J. Yu, Z. J. Liu, Y. G. Huang, K. Hwang, P. Ferreira, X. L. Li, K. Choquette and J. A. Rogers, *Science*, 2009, **325**, 977–981.
5 Z. Y. Fan, J. C. Ho, T. Takahashi, R. Yerushalmi, K. Takei, A. C. Ford, Y. L. Chueh and A. Javey, *Adv. Mater.*, 2009, **21**, 3730–3743.
6 T. H. Kim, A. Carlson, J. H. Ahn, S. M. Won, S. D. Wang, Y. G. Huang and J. A. Rogers, *Appl. Phys. Lett.*, 2009, **94**, 113502.
7 H. Ko, K. Takei, R. Kapadia, S. Chuang, H. Fang, P. W. Leu, K. Ganapathi, E. Plis, H. S. Kim, S. Y. Chen, M. Madsen, A. C. Ford, Y. L. Chueh, S. Krishna, S. Salahuddin and A. Javey, *Nature*, 2010, **468**, 286–289.
8 S. Kim, J. A. Wu, A. Carlson, S. H. Jin, A. Kovalsky, P. Glass, Z. J. Liu, N. Ahmed, S. L. Elgan, W. Q. Chen, P. M. Ferreira, M. Sitti, Y. G. Huang and J. A. Rogers, *Proc. Natl. Acad. Sci. U. S. A.*, 2010, **107**, 17095–17100.
9 C. E. Packard, A. Murarka, E. W. Lam, M. A. Schmidt and V. Bulovic, *Adv. Mater.*, 2010, **22**, 1840–1844.
10 C. C. Wu, C. H. Liu and Z. H. Zhong, *Nano Lett.*, 2010, **10**, 1032–1036.
11 H. P. Liu, D. Takagi, S. Chiashi and Y. Homma, *ACS Nano*, 2010, **4**, 933–938.
12 J. D. Caldwell, T. J. Anderson, J. C. Culbertson, G. G. Jernigan, K. D. Hobart, F. J. Kub, M. J. Tadjer, J. L. Tedesco, J. K. Hite, M. A. Mastro, R. L. Myers-Ward, C. R. Eddy, P. M. Campbell and D. K. Gaskill, *ACS Nano*, 2010, **4**, 1108–1114.
13 Y. Qi, J. Kim, T. D. Nguyen, B. Lisko, P. K. Purohit and M. C. McAlpine, *Nano Lett.*, 2011, **11**, 1331–1336.
14 A. Carlson, H. J. Kim-Lee, J. Wu, P. Elvikis, H. Y. Cheng, A. Kovalsky, S. Elgan, Q. M. Yu, P. M. Ferreira, Y. G. Huang, K. T. Turner and J. A. Rogers, *Appl. Phys. Lett.*, 2011, **98**, 264104.
15 J. Wu, S. Kim, W. Q. Chen, A. Carlson, K. C. Hwang, Y. G. Huang and J. A. Rogers, *Soft Matter*, 2011, **7**, 8657–8662.
16 R. Saeidpourazar, R. Li, Y. Li, M. D. Sangid, C. F. Lü, Y. Huang, J. A. Rogers and P. M. Ferreira, *J. Microelectromech. Syst.*, 2012, (to appear).
17 A. Nathan, B. Park, A. Sazonov, S. Tao, I. Chan, P. Servati, K. Karim, T. Charania, D. Striakhilev, Q. Ma and R. V. R. Murthy, *Microelectron. J.*, 2000, **31**, 883–891.
18 V. J. Lumelsky, M. S. Shur and S. Wagner, *IEEE Sens. J.*, 2001, **1**, 41–51.
19 S. C. B. Mannsfeld, B. C. K. Tee, R. M. Stoltenberg, C. V. H. H. Chen, S. Barman, B. V. O. Muir, A. N. Sokolov, C. Reese and Z. N. Bao, *Nat. Mater.*, 2010, **9**, 859–864.
20 T. Someya, Y. Kato, T. Sekitani, S. Iba, Y. Noguchi, Y. Murase, H. Kawaguchi and T. Sakurai, *Proc. Natl. Acad. Sci. U. S. A.*, 2005, **102**, 12321–12325.
21 T. Someya and T. Sekitani, *Procedia Chem.*, 2009, **1**, 9–12.

22 G. P. Crawford, *Flexible Flat Panel Display Technology*, Wiley, New York, 2005.
23 S. R. Forrest, *Nature*, 2004, **428**, 911–918.
24 G. H. Gelinck, H. E. A. Huitema, E. Van Veenendaal, E. Cantatore, L. Schrijnemakers, J. B. P. H. Van der Putten, T. C. T. Geuns, M. Beenhakkers, J. B. Giesbers, B. H. Huisman, E. J. Meijer, E. M. Benito, F. J. Touwslager, A. W. Marsman, B. J. E. Van Rens and D. M. De Leeuw, *Nat. Mater.*, 2004, **3**, 106–110.
25 D. H. Kim, J. H. Ahn, W. M. Choi, H. S. Kim, T. H. Kim, J. Z. Song, Y. G. Y. Huang, Z. J. Liu, C. Lu and J. A. Rogers, *Science*, 2008, **320**, 507–511.
26 T. Sekitani, U. Zschieschang, H. Klauk and T. Someya, *Nat. Mater.*, 2010, **9**, 1015–1022.
27 J. Yoon, A. J. Baca, S. I. Park, P. Elvikis, J. B. Geddes, L. F. Li, R. H. Kim, J. L. Xiao, S. D. Wang, T. H. Kim, M. J. Motala, B. Y. Ahn, E. B. Duoss, J. A. Lewis, R. G. Nuzzo, P. M. Ferreira, Y. G. Huang, A. Rockett and J. A. Rogers, *Nat. Mater.*, 2008, **7**, 907–915.
28 T. Sekitani, H. Nakajima, H. Maeda, T. Fukushima, T. Aida, K. Hata and T. Someya, *Nat. Mater.*, 2009, **8**, 494–499.
29 T. Someya, T. Sekitani, S. Iba, Y. Kato, H. Kawaguchi and T. Sakurai, *Proc. Natl. Acad. Sci. U. S. A.*, 2004, **101**, 9966–9970.
30 H. C. Ko, M. P. Stoykovich, J. Z. Song, V. Malyarchuk, W. M. Choi, C. J. Yu, J. B. Geddes, J. L. Xiao, S. D. Wang, Y. G. Huang and J. A. Rogers, *Nature*, 2008, **454**, 748–753.
31 D. H. Kim, J. Viventi, J. J. Amsden, J. L. Xiao, L. Vigeland, Y. S. Kim, J. A. Blanco, B. Panilaitis, E. S. Frechette, D. Contreras, D. L. Kaplan, F. G. Omenetto, Y. G. Huang, K. C. Hwang, M. R. Zakin, B. Litt and J. A. Rogers, *Nat. Mater.*, 2010, **9**, 511–517.
32 J. Viventi, D. H. Kim, J. D. Moss, Y. S. Kim, J. A. Blanco, N. Annetta, A. Hicks, J. L. Xiao, Y. G. Huang, D. J. Callans, J. A. Rogers and B. Litt, *Sci. Transl. Med.*, 2010, **2**, 24ra22.
33 D. H. Kim, N. S. Lu, R. Ghaffari, Y. S. Kim, S. P. Lee, L. Z. Xu, J. A. Wu, R. H. Kim, J. Z. Song, Z. J. Liu, J. Viventi, B. de Graff, B. Elolampi, M. Mansour, M. J. Slepian, S. Hwang, J. D. Moss, S. M. Won, Y. G. Huang, B. Litt and J. A. Rogers, *Nat. Mater.*, 2011, **10**, 316–323.
34 J. Viventi, D. H. Kim, L. Vigeland, E. S. Frechette, J. A. Blanco, Y. S. Kim, A. E. Avrin, V. R. Tiruvadi, S. W. Hwang, A. C. Vanleer, D. F. Wulsin, K. Davis, C. E. Gelber, L. Palmer, J. Van der Spiegel, J. Wu, J. L. Xiao, Y. G. Huang, D. Contreras, J. A. Rogers and B. Litt, *Nat. Neurosci.*, 2011, **14**, 1599–1605.
35 R. H. Kim, D. H. Kim, J. L. Xiao, B. H. Kim, S. I. Park, B. Panilaitis, R. Ghaffari, J. M. Yao, M. Li, Z. J. Liu, V. Malyarchuk, D. G. Kim, A. P. Le, R. G. Nuzzo, D. L. Kaplan, F. G. Omenetto, Y. G. Huang, Z. Kang and J. A. Rogers, *Nat. Mater.*, 2010, **9**, 929–937.
36 D. H. Kim, N. S. Lu, R. Ma, Y. S. Kim, R. H. Kim, S. D. Wang, J. Wu, S. M. Won, H. Tao, A. Islam, K. J. Yu, T. I. Kim, R. Chowdhury, M. Ying, L. Z. Xu, M. Li, H. J. Chung, H. Keum, M. McCormick, P. Liu, Y. W. Zhang, F. G. Omenetto, Y. G. Huang, T. Coleman and J. A. Rogers, *Science*, 2011, **333**, 838–843.
37 F. P. Incropera, D. P. DeWitt, T. L. Bergman and A. S. Lavine, *Fundamentals of Heat and Mass Transfer*, Wiley, Hoboken, 2007.
38 S. A. Campbell, *The Science and Engineering of Microelectronic Fabrication*, Oxford University Press, New York, 2001.
39 ed. J. E. Mark, *Polymer Data Handbook*, Oxford University Press, New York, 1999.
40 H. E. Fettis, J. C. Caslin and K. R. Cramer, *Math. Comput.*, 1973, **27**, 401–407.
41 ABAQUS Analysis User's Manual V6.9, Dassault Systèmes, Pawtucket, 2009.
42 Y. Okada and Y. Tokumaru, *J. Appl. Phys.*, 1984, **56**, 314–320.
43 Z. G. Suo, *Int. J. Solids Struct.*, 1989, **25**, 1133–1142.

Addition and correction

Note from RSC Publishing

This article was originally published with incorrect page numbers. This is the corrected, final version.

The Royal Society of Chemistry apologises for these errors and any consequent inconvenience to authors and readers.